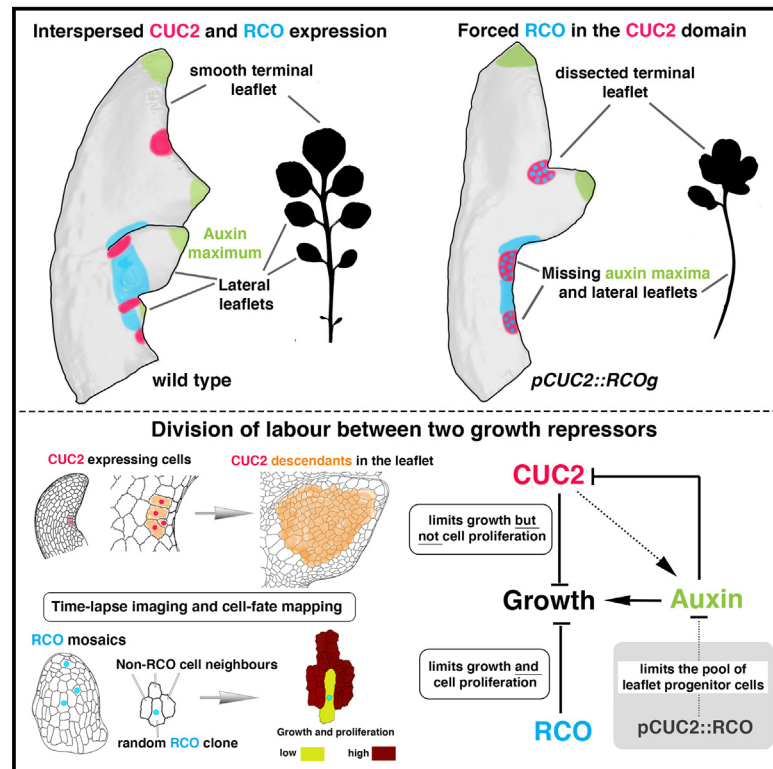


Current Biology

Interspersed expression of *CUP-SHAPED COTYLEDON2* and *REDUCED COMPLEXITY* shapes *Cardamine hirsuta* complex leaf form

Graphical abstract



Authors

Neha Bhatia, David Wilson-Sánchez, Sören Strauss, ..., Ziliang Hu, Léa Rambaud-Lavigne, Miltos Tsiantis

Correspondence

tsiantis@mpipz.mpg.de

In brief

Bhatia et al. use time-lapse imaging, genetic perturbations, and cellular growth analysis to show that spatially separated growth-repressive activities of *CUC2* and *RCO* shape *C. hirsuta* complex leaf form. They find different relationships between cell proliferation and growth repression during patterning and post-patterning stages of organogenesis.

Highlights

- *CUC2* and *RCO* are expressed in an interspersed pattern in *C. hirsuta* complex leaves
- This interspersed expression is required for complex leaf development
- *RCO* limits both cell proliferation and cellular growth in a cell-autonomous manner
- The cellular parameters for growth repression by *CUC2* and *RCO* are distinct

Article

Interspersed expression of *CUP-SHAPED COTYLEDON2* and *REDUCED COMPLEXITY* shapes *Cardamine hirsuta* complex leaf form

Neha Bhatia,¹ David Wilson-Sánchez,¹ Sören Strauss,¹ Francesco Vuolo,^{1,2} Bjorn Pieper,¹ Ziliang Hu,¹ Léa Rambaud-Lavigne,^{1,3} and Miltos Tsiantis^{1,4,*}

¹Department of Comparative Development and Genetics, Max Planck Institute for Plant Breeding Research, Carl-von-Linné-Weg 10, 50829 Cologne, Germany

²Present address: Sacco srl, Via Alessandro Manzoni 29/A, 22071 Cadorago, CO, Italy

³Present address: Laboratoire de Reproduction et Développement des Plantes, ENS de Lyon46, allée d'Italie, 69364 Lyon Cedex 07, France

⁴Lead contact

*Correspondence: tsiantis@mpipz.mpg.de

<https://doi.org/10.1016/j.cub.2023.06.037>

SUMMARY

How genetically regulated growth shapes organ form is a key problem in developmental biology. Here, we investigate this problem using the leaflet-bearing complex leaves of *Cardamine hirsuta* as a model. Leaflet development requires the action of two growth-repressing transcription factors: *REDUCED COMPLEXITY* (*RCO*), a homeodomain protein, and *CUP-SHAPED COTYLEDON2* (*CUC2*), a NAC-domain protein. However, how their respective growth-repressive actions are integrated in space and time to generate complex leaf forms remains unknown. By using live imaging, we show that *CUC2* and *RCO* are expressed in an interspersed fashion along the leaf margin, creating a distinctive striped pattern. We find that this pattern is functionally important because forcing *RCO* expression in the *CUC2* domain disrupts auxin-based marginal patterning and can abolish leaflet formation. By combining genetic perturbations with time-lapse imaging and cellular growth quantifications, we provide evidence that *RCO*-mediated growth repression occurs after auxin-based leaflet patterning and in association with the repression of cell proliferation. Additionally, through the use of genetic mosaics, we show that *RCO* is sufficient to repress both cellular growth and proliferation in a cell-autonomous manner. This mechanism of growth repression is different to that of *CUC2*, which occurs in proliferating cells. Our findings clarify how the two growth repressors *RCO* and *CUC2* coordinate to subdivide developing leaf primordia into distinct leaflets and generate the complex leaf form. They also indicate different relationships between growth repression and cell proliferation in the patterning and post-patterning stages of organogenesis.

INTRODUCTION

How different gene activities integrate to orchestrate spatio-temporal coordination of cell and tissue growth during morphogenesis is a key question in developmental biology.¹ Plant leaves are an attractive system to study this problem because they show complex and diverse leaf shapes and their morphogenesis is free of cell migration, which allows a clear appreciation of the effects of genetically regulated growth on form. A key feature of leaf shape is the generation of repeated marginal protrusions; for example, tooth-like serrations in the simple leaves of *Arabidopsis thaliana* (*A. thaliana*) and separated units—called leaflets—in its relative, *Cardamine hirsuta* (*C. hirsuta*). Leaf shape emerges through an interplay between distributed growth-regulating gene activities, signaling, cell proliferation, and differentiation. The net outcome of this interplay, which is also modified by mechanical interconnections between cells, is a given amount, duration, and direction of growth that ultimately

shapes leaf form.¹ Contributions from programmed cell death are rare and species-specific.² A recent study showed that two evolutionary conserved growth mechanisms are important for leaf shape: an organ-wide mechanism that controls the duration of growth in association with modulating differentiation and a local mechanism that controls the patterning of outgrowths along the leaf margin.³ The latter comprises a small genetic network involving the growth-promoting plant hormone, auxin; its transport, mediated by the auxin efflux protein PIN FORMED 1 (*PIN1*); and a growth-repressing transcription-factor, *CUP-SHAPED COTYLEDON2* (*CUC2*), that belongs to the NAC-domain (*NO APICAL MERISTEM* (*NAM*); *ATAF1,2* and *CUC2*) family.^{4,5} This genetic network drives periodic outgrowth formation along the leaf margin.^{6–8} This patterning process distributes foci of lateral, anisotropic growth, mediated by auxin signaling, at the tip of initiating protrusions and foci of growth repression, mediated by *CUC2*, at the base of initiating protrusions, where it is expressed.^{3,7}

Crucifers, including *C. hirsuta*, have evolved an additional growth repressor, *REDUCED COMPLEXITY* (*RCO*), which encodes a class I HOMEODOMAIN LEUCINE ZIPPER (HD-ZIP I) transcription factor.^{9,10} Similar to *CUC2*, *RCO* is also expressed at the base of initiating leaflets in *C. hirsuta*, where it is required to suppress growth locally, thus helping create complex leaves through leaflet separation. Loss of *RCO* from the *A. thaliana* genome contributed to leaf simplification, and introducing *RCO* as a transgene resulted in increased complexity in *A. thaliana* leaves.¹⁰ Together, these results suggest that *RCO* is an important driver of leaf shape diversity within crucifers. However, the precise cellular mechanisms through which it affects growth to sculpt complex leaf forms are poorly understood. It has been proposed that *RCO* may act during post-patterning stages¹¹ of leaf development to repress growth at the base of emerging leaflets after their initiation by the *CUC*-auxin based patterning system.¹⁰ *CUC* genes, on the other hand, play a dual role in mediating the long-range organization of auxin-transport-dependent auxin activity maxima, which mark leaflet initiation sites and increase growth locally at leaflet tips while also repressing growth at leaflet bases to delimit separate leaflets. How the action of these two growth repressors is integrated in space and time remains unclear. This presents a key problem in understanding how genetically regulated growth shapes complex leaf form.

RESULTS AND DISCUSSION

Interspersed *RCO* and *CUC2* expression resolves in a striped pattern

To understand how activities of *CUC2* and *RCO* are integrated during *C. hirsuta* complex leaf development, we sought to obtain fine-grained information about their relative gene expression domains in space and time. To this end, we simultaneously imaged a *CUC2* translational reporter (*pChCUC2::ChCUC2g-VENUS*), together with a nuclear localized *RCO* transcriptional reporter (*pRCO::nls-tdTomato*), within developing *C. hirsuta* leaf primordia. We found that *pChCUC2::ChCUC2g-VENUS* expression preceded *pRCO::nls-tdTomato* expression, both during leaf emergence and lateral leaflet (LL) initiation at the leaf margin (Figures S1A–S1L). Notably, only *pChCUC2::ChCUC2g-VENUS* and not *pRCO::nls-tdTomato* expression was detected at the LL initiation site along the leaf margin (yellow arrowheads in Figures S1G–S1L). We detected *RCO* expression in *p35S::MIR164B*; *CUC3RNAi* double transgenic lines, which show reduced *CUC1-3* expression,⁸ indicating that *CUC* genes are unlikely to be strictly required for *RCO* expression in the *C. hirsuta* leaf margin (Video S1). Together, these results indicate that *RCO* might act independently of *CUC2* and predominantly post-patterning to shape leaf form. As the final leaf shape emerged, two striking differences between *CUC2* and *RCO* expression became apparent (Figures 1A–1C). (1) *pChCUC2::ChCUC2g-VENUS* expresses in the distal domains of the terminal leaflet (TL), with expression foci in the sinus regions of TL protrusions (Figure 1B, white arrowheads). In contrast to this, *pRCO::nls-tdTomato* does not express in the TL, but rather at the junction between the TL and the first

LL (Figure 1A, yellow arrowhead). (2) *pRCO::nls-tdTomato* expression is interspersed among narrow stripes of *pChCUC2::ChCUC2g-VENUS* expression that lie on the distal side of LL bases (Figures 1A–1C) along the rachis. A quantitative estimation of the signal intensity of one reporter in the domain of the other at LL bases indicated significantly lower levels of *pRCO::nls-tdTomato* signal intensity in the *pChCUC2::ChCUC2g-VENUS* domain than the *pRCO::nls-tdTomato* domain and vice versa (Figures 1D–1F). This further indicates the occurrence of separate expression domains of *CUC2* and *RCO* at LL bases. Additionally, we examined the expression pattern of a rescuing *RCO* translational reporter (*pRCO::RCOg-YPet-3'utr*) and found a similar discontinuous spatial distribution as for *pRCO::nls-tdTomato* (Video S2, white arrowheads), albeit more restricted, perhaps due to negative autoregulation¹² or post transcriptional regulation. Together, these results suggest that although two growth repressors, *RCO* and *CUC2*, are both expressed at the base of leaflets in a discontinuous manner, their expression foci are largely kept separate in space and time during complex leaf morphogenesis in *C. hirsuta*.

RCO expression in the *CUC2* domain perturbs leaf marginal patterning and form

To evaluate whether the observed separation of the expression domains of these two growth repressive genes has functional relevance for complex leaf development, we disrupted their interspersed expression. For this, we expressed *RCO* genomic or coding sequences under the control of *CUC2* 5' regulatory sequences (*pCUC2::RCO*) from either *A. thaliana* or *C. hirsuta*. This is predicted to result in a near-continuous expression of *RCO* along the leaf margin because the two genes are expressed in a near-complementary fashion. We found that forcing *RCO* expression in the *CUC2* domain in this way resulted in a highly modified leaf shape with two striking phenotypes (Figures 2A and S2A–S2D). First, we observed a highly dissected TL, as also indicated by an increase in the normalized marginal differential complexity (NDMC) relative to wild type (Figures 2A and 2C). This phenotype is consistent with the expression of *RCO* in the sinuses of the TL protrusions, where the promoter of *CUC2*—but not *RCO*—is active. Second, we observed a significant reduction in the number of LLs in plants expressing *pCUC2::RCO*, resulting in narrow leaves compared with wild-type plants (Figures 2A and 2B). To investigate whether *pCUC2::RCO* may cause this phenotype through interfering with the marginal patterning system or disrupted growth of LLs post-patterning, we examined expression of the auxin activity sensor *pDR5v2::nls-3xVENUS*.¹³ We did not detect *pDR5v2::nls-3xVENUS* maxima at LL initiation sites, suggesting that *pCUC2::RCO* perturbed auxin signaling along the leaf margin (Figures 2D and 2E). In summary, we observed that the near-continuous and precocious *RCO* expression that arises from forcing *RCO* in the *CUC2* domain is sufficient to abolish auxin activity maxima and LLs. Therefore, we conclude that interspersed expression of *CUC2* and *RCO* is required to establish periodic auxin-signaling maxima that guide LL initiation and outgrowth.

It was previously shown that auxin-based patterning, as monitored by the generation of sequential DR5 peaks, is intact

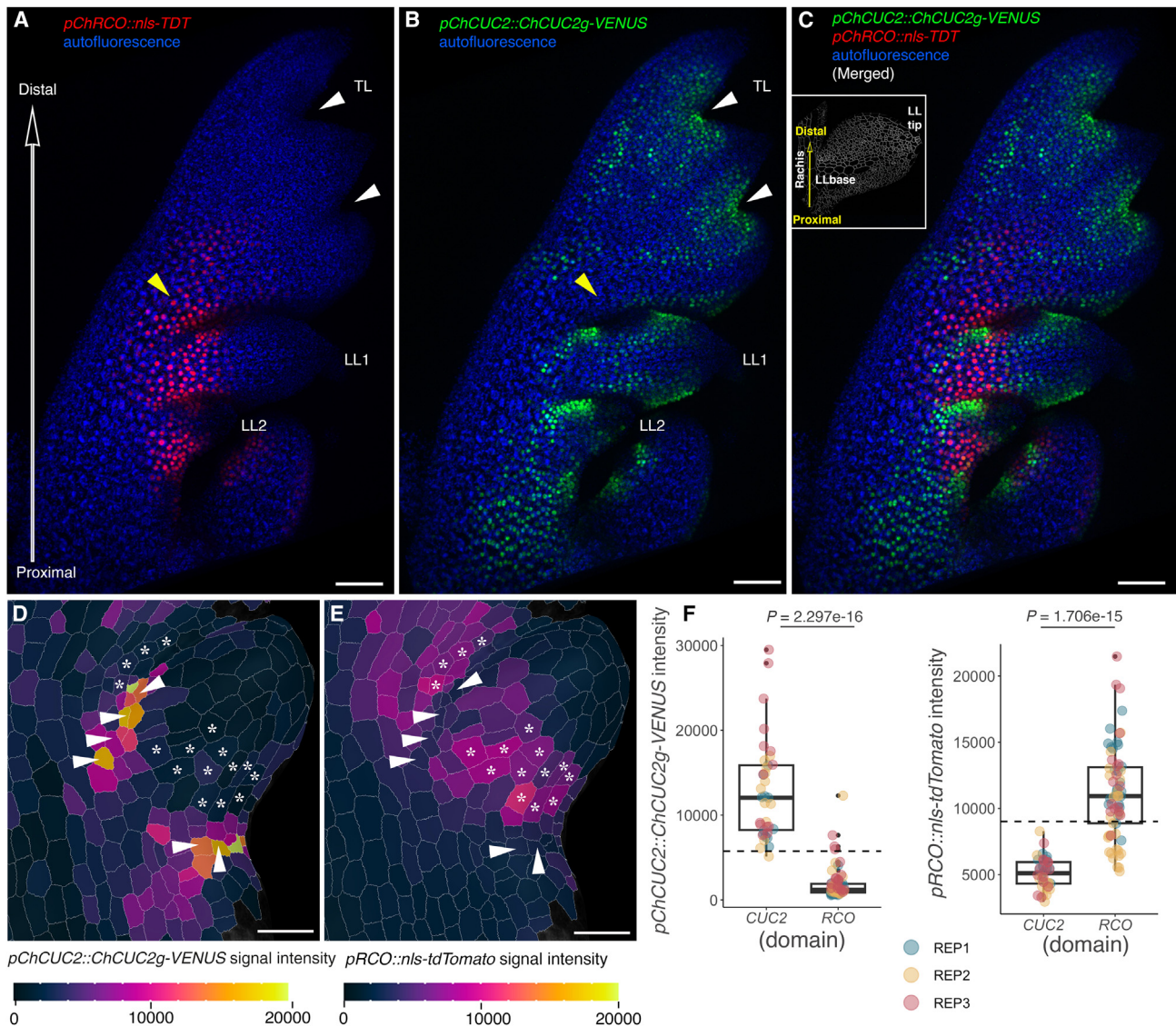


Figure 1. *RCO* and *CUC2* expression are interspersed along the leaf margin

(A–C) Confocal projections of *C. hirsuta* wild-type leaf 7 showing expression of *pRCO::nls-tdTomato* (red) (A), *pChCUC2::ChCUC2g-VENUS* (green) (B), and *pChCUC2::ChCUC2g-VENUS* and *pRCO::nls-tdTomato* together (C). White arrowheads in (A) and (B) indicate the presence of *pChCUC2::ChCUC2g-VENUS* (B) and absence of *pRCO::nls-tdTomato* in sinus regions of the TL (A). Yellow arrowheads in (A) and (B) indicate the presence of *pRCO::nls-tdTomato* and absence of *pChCUC2::ChCUC2g-VENUS* at the base of the terminal leaflet ($n = 7$ leaves, 2 independent transgenic lines). Inset in (C) shows a developing lateral leaflet (LL) and highlights its tip to base (proximo-distal) axis relative to the proximo-distal axis of the rachis.

(D and E) Magnified views of wild-type LL of leaf 6 showing heatmaps of *pChCUC2::ChCUC2g-VENUS* (D) and *pRCO::nls-tdTomato* (E) signal intensities. White arrowheads in (D) and (E) mark cells with high *pChCUC2::ChCUC2g-VENUS* intensity in (D) and same cells showing low *pRCO::nls-tdTomato* intensity in (E). White asterisks in (D) and (E) mark cells with high *pRCO::nls-tdTomato* signal intensity in (E) and same cells showing low *pChCUC2::ChCUC2g-VENUS* intensity in (D). (F) Dot boxplots showing quantifications of *pChCUC2::ChCUC2g-VENUS* and *pRCO::nls-tdTomato* signal intensities in *pChCUC2::ChCUC2g-VENUS* and *pRCO::nls-tdTomato* expression domains (Kruskal-Wallis non-parametric test, $n = 3$). The significance threshold used was $P < 0.05$. Scale bars, 50 μm (A–C) and 20 μm (D and E). TL, terminal leaflet; LL, lateral leaflet; *Ch*, *C. hirsuta*.

See also [Figure S1](#) and [Videos S1](#) and [S2](#).

along the leaf margins of *rco* loss-of-function mutants.¹⁰ Therefore, we sought to understand the functional significance of the *RCO* expression domain at developing LL bases relative to leaflet outgrowth. To this end, we introduced *pChCUC2::RCO_{cds}-YPet* as a transgene in *rco* mutants to test whether *RCO* expression in the more distal *CUC2* domain, as opposed to its endogenous domain at the base of emerging

LLs, would be sufficient to restore LL formation. *RCO_{cds}-YPet* under the control of the *RCO* promoter (*pRCO::RCO_{cds}-YPet*) fully complemented the *rco* mutant phenotype, forming complex leaves with a separated, smooth TL and distinct, petiolulated LLs ([Figures 3A–3C](#)). However, the leaf shapes of *rco* mutants expressing *pChCUC2::RCO_{cds}-YPet* were clearly distinct from wild type and showed increased dissection of the TL and two

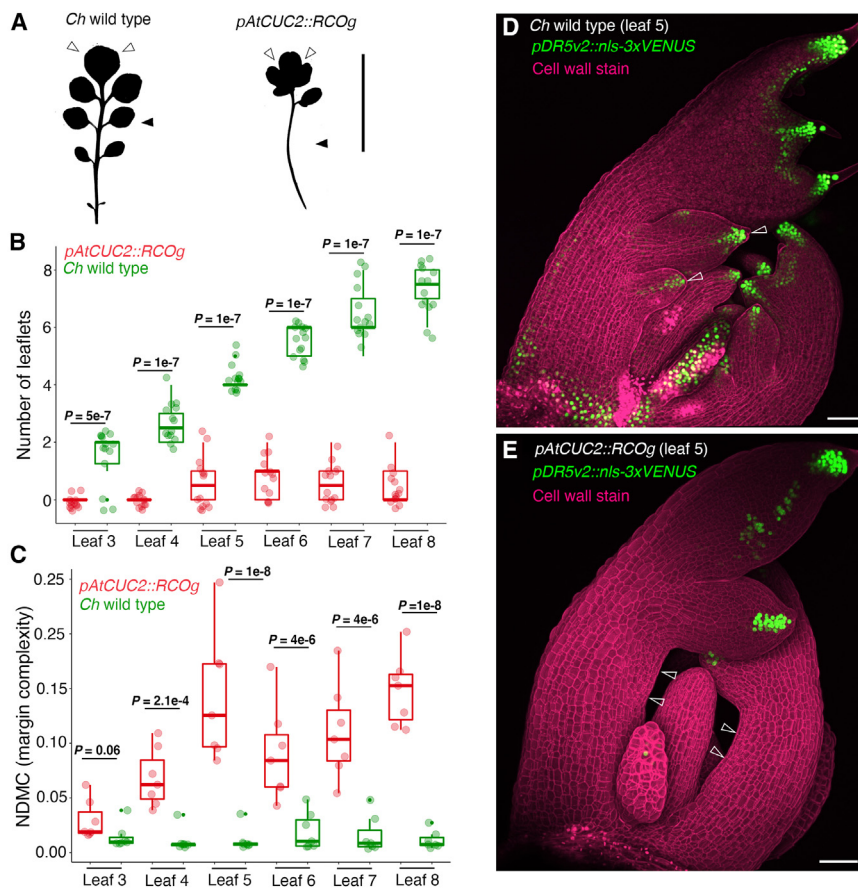


Figure 2. Forced RCO expression in the CUC2 domain alters leaf form and disrupts marginal patterning

(A) Silhouettes of leaf 7 of *C. hirsuta* wild type and wild type carrying *pAtCUC2::RCOg* transgene (referred to as *pAtCUC2::RCOg* hereafter). Note a lobed TL in *pAtCUC2::RCOg* genotype compared with a smooth TL in the wild type (white arrowheads) and a reduction in LLs in *pAtCUC2::RCOg* genotype ($n = 3$ T2 transgenic lines) relative to wild type (black arrowheads).

(B) Quantification of LL number in leaf nodes 3–8 of *Ch* wild type and *pAtCUC2::RCOg* ($n = 14$ plants). (C) Quantification of TL marginal complexity in leaf nodes 3–8 of *Ch* wild type and *pAtCUC2::RCOg* ($n = 7$ plants). Statistical significance in (B) and (C) was tested using ANOVA followed by Tukey's honestly significant difference test (Tukey's HSD) for pairwise comparison with a significance threshold of $P < 0.05$.

(D and E) Confocal projections of leaf 5 of *Ch* wild type (D) and *pAtCUC2::RCOg* showing expression of *pDR5v2::nls-3xVENUS* (green) and cell wall stain (magenta). White arrowheads indicate the presence *pDR5v2::nls-3xVENUS*-maxima along the leaf margin of wild type and their absence in *pAtCUC2::RCOg* ($n = 3$, wild type; $n = 7$, *pAtCUC2::RCOg*). Scale bars, 5 cm (A), 50 μm (D and E). *Ch*, *C. hirsuta*; *At*, *A. thaliana*; LL, lateral leaflet; TL, terminal leaflet.

See also Figure S2.

classes of transgene-expression-dependent LL phenotypes (Figures 3A–3D and S2E). (1) LLs lacking a distinct petiole, which was fused to the rachis, and (2) absence or reduction in LL number. We also found a significant increase in the presence of intercalary leaflets, as well as irregularities in the inter-rachis length, in *rco* mutants expressing *pChCUC2::RCO_{cds}-YPet* (Figures 3E and 3F). These irregular LL positioning defects correlated with a deviation in the spacing of marginal auxin activity maxima, reported by *pDR5v2::nls-tdTomato*, compared with wild type (Figures 3G–3I), indicating that auxin-based patterning is disrupted by *pChCUC2::RCO_{cds}-YPet*. These findings help explain why *RCO* is expressed medio-proximally rather than distally at the base of emerging LLs and later than *CUC2*. Although a discontinuous expression of *RCO* on either side of the LL base is sufficient to generate distinct leaflets, *RCO* needs to be restricted to medio-proximal regions, separated from the distal *CUC2*-auxin-based patterning domain, in order to minimize its potentially detrimental effects on the periodic spacing of auxin activity maxima.

RCO is necessary and sufficient to limit both cellular growth and proliferation, cell autonomously

We next investigated the cellular effects through which *RCO* causes a modified leaf shape in *pCUC2::RCOg* plants. For this, we used time-lapse imaging and cell-fate mapping to compute organ-wide patterns of cellular growth in the developing leaves of wild-type, *rco* loss-of-function, and

pAtCUC2::RCOg gain-of-function contexts (Video S3). We found a strong reduction in cell proliferation and cell area extension along the leaf margins of wild-type leaves expressing *pAtCUC2::RCOg* (white arrowheads in Figures 4A and 4B) compared with wild-type and *rco* mutants (Figures 4C–4F and S3A–S3D). We next analyzed cellular growth patterns in the sinus regions of the TL of *pAtCUC2::RCOg* and wild-type plants and identified a localized zone of highly reduced cell proliferation and cell area extension in the TL sinus regions of *pAtCUC2::RCOg* leaves compared with wild type (Figures 4G–4N). These findings indicate that *RCO*-mediated repression of cell growth and proliferation along the leaf margin and in the sinus region of the TL underpins reduced leaflet outgrowth and dissection of the TL in *pCUC2::RCO*-expressing plants, respectively. Rather than primordium-wide growth differences (Figures S3C and S3D), we found a local increase in cell proliferation and cell area extension in *rco* mutants compared with wild type at the junctions between TL and first LL, as well as between two LLs (white arrowheads, dotted outlines in Figures S3E–S3H), where *RCO* is normally expressed (Figure 1A). This increased growth in junctions between TL and first LL and between two LLs due to lack of *RCO* activity in those regions explains the failure of leaflet separation in the *rco* mutants, consistent with previous observations.¹⁰ Altogether, these findings suggest that *RCO* is both necessary and sufficient to limit cell proliferation and growth, and its action may be restricted to its domain of expression.

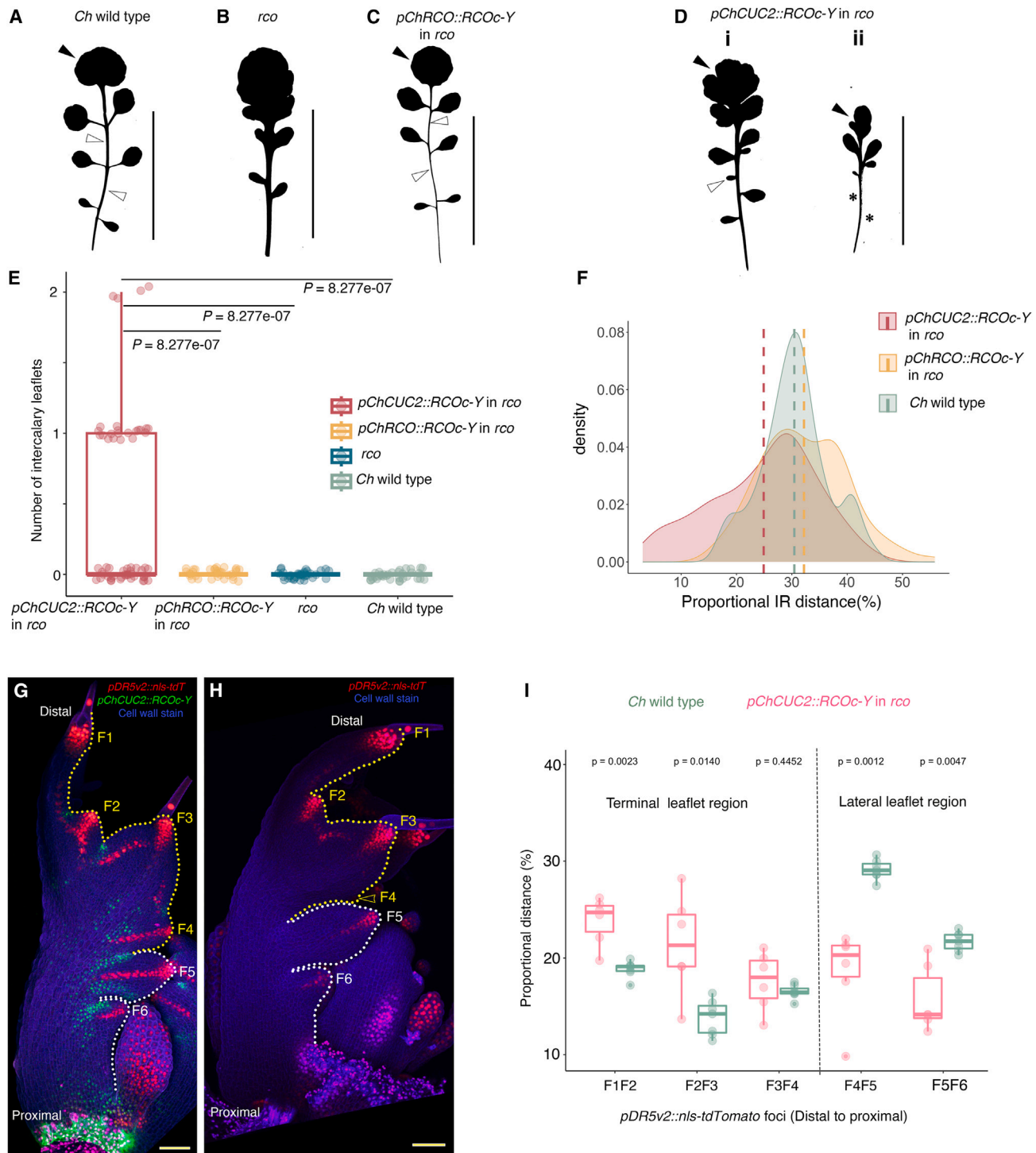


Figure 3. *pCUC2::RCO* partially restores leaflet formation in *rco* mutants but perturbs leaflet spacing

(A–C) Silhouettes of leaf 7 of *C. hirsuta* wild type (A), *rco* mutant (B), and *rco* mutant carrying *pRCO::RCO_{cds}-YPet*, (n = 2 T2 transgenic lines). (D) Silhouettes of leaf 7 of *rco* mutant carrying *pChCUC2::RCO_{cds}-YPet* showing two different phenotypes—LLs lacking a distinct petiolule, which was fused to the rachis (Di; n = 8 independent T2 transgenic lines) and absence or reduction in LL number (Dii; n = 2 T2 transgenic lines). White arrowheads indicate the presence of intercalary leaflets (ILs) in (Di) and their absence in (A) and (C). Asterisks in (Dii) indicate reduction in LLs. Black arrowheads in (A), (C), and (D) indicate increased dissection of the TL in *rco* mutants carrying *pChCUC2::RCO_{cds}-YPet*, compared with wild-type and *rco* mutants carrying *pRCO::RCO_{cds}-YPet*. (E) Quantification of number of ILs in *Ch* wild type, *rco* mutant, *rco* mutant carrying *pRCO::RCO_{cds}-YPet* (n = ~30 plants from 2 T2 lines, with 15 plants from each line), and *rco* mutant carrying *pChCUC2::RCO_{cds}-YPet*; n = ~33 plants from 4 independent T2 lines with 8 plants from each line in (Di); statistical significance was tested using Kruskal-Wallis followed by Dunn's post hoc test with a significance threshold of $P < 0.05$.

(legend continued on next page)

To further test the sufficiency of *RCO* to limit growth in association with limiting cell proliferation, and to determine the range of *RCO* action, we utilized *Cre-lox* recombination¹⁴ to generate mosaics of *RCO_{cds}-YPet*-expressing cells within the developing leaves of *A. thaliana*, which lack *RCO* activity (Figures 5A and S4). This method results in the juxtaposition of wild-type cells and genetically modified cells randomly within a tissue. Consequently, it is a powerful tool for studying the cellular underpinnings and the range of growth repression conferred by *RCO*. We performed time-lapse imaging and computed cell-fate maps in leaves where we induced *RCO_{cds}-YPet* mosaics as well as in control leaves (Figures 5B, 5Bi–5Biii, 5C, and 5Ci–5Ciii). Our results show that *RCO_{cds}-YPet* reduces cell proliferation and growth in cells where it is expressed, compared with cells at equivalent positions in the control that lack *RCO_{cds}-YPet* (Figures 5D–5G and S4A–S4H), in a cell-autonomous manner (white arrowheads in Figures 5D, 5F, S4I, and S4J). In conclusion, *RCO* is necessary and sufficient to reduce growth and cell proliferation where it is expressed.

Different relationship between repression of cell growth and proliferation in the *CUC2* and *RCO* domain

Our findings indicate that limiting cell proliferation is integral to *RCO*-mediated growth repression and consequent leaf dissection. This mode of growth repression appears to be different to that observed in *CUC2*-expressing cells, as those proliferate, creating a substantive pool of descendant cells (Figures S5A–S5M). Although growth can be regulated independent of proliferation,¹⁵ changes in proliferation rates can offset changes in cell size,^{15,16} and the duration of cell proliferation can influence the number of cells, which can later differentiate and grow.^{17–19} We propose that one consequence of forcing *RCO* activity in the *CUC2* patterning domain of the leaf is to limit the number of LL progenitor cells, thereby causing a reduction in LL formation in *pCUC2::RCO*-expressing plants.

In conclusion, we show that spatially separated growth-repressive activities of *CUC2* and *RCO* sculpt *C. hirsuta* complex leaf shape and that these regulators operate largely independently on the leaf margin. A distinctive feature of this system is that *RCO*-mediated growth repression occurs post-patterning and in association with the repression of cell proliferation, while *CUC2*-dependent growth repression occurs in proliferating cells during margin patterning. Our data indicates that this division of labor protects the *CUC*-auxin patterning system from the

potentially detrimental effects of *RCO* on patterning, thus ensuring that a sufficient pool of proliferative cells is generated to support the emergence of developing LL primordia (Figure S5N). The *CUC*-auxin patterning system acts in different tissues during plant development to support boundary function and promote organogenesis.^{5,20,21} In the future, it will be interesting to investigate whether slowing down growth while maintaining cell proliferation in organ boundaries is a more general feature of *CUC*-auxin-mediated organogenesis in plants. Given that *RCO* is expressed in leaves of some crucifer species but not others,²² this mode of growth repression involving *CUC* and *RCO* acting in separate domains likely allowed the exploration of broader phenotypic space by evolution to shape leaf form.

The increased lobing we observed in the TL of *C. hirsuta* plants expressing *pCUC2::RCO* is reminiscent of the lobed leaf phenotype observed in *A. thaliana* simple leaves carrying an *RCO* transgene expressed under its endogenous (*C. hirsuta*) regulatory sequence.¹⁰ In light of these findings, it is tempting to revisit one view on comparative consideration of simple and complex leaves, according to which the *A. thaliana* simple leaf corresponds to the TL rather than the entire complex leaf of *C. hirsuta*.²³ According to this view, leaf simplification, which is a derived feature in *A. thaliana*, would have occurred through deletion of the LL—producing proximal organogenetic zone of complex leaves—the rachis. However, in *A. thaliana* strains harboring the same *RCO* transgene,¹⁰ *RCO* is expressed at the base of initiating serrations, thus mirroring its expression in *C. hirsuta*, where it is expressed at the base of developing leaflets at the rachis.¹⁰ Therefore, it is unlikely that the loss of complexity in *A. thaliana* leaves merely reflects an evolutionary loss of the LL-producing domain of complex leaves. Rather, our data is consistent with the idea that the *A. thaliana* leaf retains at its base aspects of the genetic program normally expressed in the *C. hirsuta* rachis and that the loss of *RCO*-mediated accentuation of growth differences created by auxin-based marginal patterning contributed to leaf simplification in the *A. thaliana* lineage.

Our findings also highlight a potentially unifying mechanism of development in multicellular eukaryotes. Namely, that the regulated maintenance of cell proliferation in progenitor cells is important to give rise to repeated tissue units, such as digits in the limb bud, teeth from tooth germs, and leaflets in complex leaves. Forced *RCO* expression in the *CUC2*-patterning domain limits proliferation of the LL progenitor cells and causes a reduction in the number of LLs. Similarly,

(F) A density plot showing distribution of proportional IR distances in leaf nodes 7 and 8 in wild type (green, $n = 12$ leaves; 6 plants), *pRCO::RCO_{cds}-YPet* in *rco* (yellow, $n = 32$ leaves from 2 T2 lines with 8 plants each), and *pChCUC2::RCO_{cds}-YPet* in *rco* (red, $n = \sim 64$ leaves from 4 T2 lines in (Di) with 8 plants each). A two-sided Kolmogorov-Smirnov test with a significance threshold of $P < 0.05$ showed that the distribution of proportional IR distances in *pChCUC2::RCO_{cds}-YPet*, *rco* was different to wild type ($P = 0.0005501$), while that of *pChRCO::RCO_{cds}-YPet*, *rco* was not ($P = 0.1248$).

(G) Confocal projection of *rco* mutant leaf 6 showing expression of *pChCUC2::RCO_{cds}-YPet* (green), *pDR5v2::nls-tdTomato* (red) and chlorophyll autofluorescence (blue).

(H) Confocal projection of *Ch* wild-type leaf 6 showing expression *pDR5v2::nls-tdTomato* (red) and chlorophyll autofluorescence (blue). *pDR5v2::nls-tdTomato* expression foci are marked as F1–F6 (not in the sequential order of their origin). Yellow dotted lines outline the TL and white dotted lines outline LLs.

(I) Quantifications of measurement of distance between *pDR5v2::nls-tdTomato* expression foci in *rco* mutants expressing *pChCUC2::RCO_{cds}-YPet* and *Ch* wild type shown in (G) and (H) ($n = 6$ leaves each). Note an increased distance between *pDR5v2::nls-tdTomato* expression foci in the TL of *rco* mutants expressing *pChCUC2::RCO_{cds}-YPet* compared with the wild type. Also note a reduction in the distance between *pDR5v2::nls-tdTomato* foci in the LLs, correlating with irregular LL positioning, compared with wild type (also see STAR Methods). Statistical validation was performed using Wilcoxon test with a significance threshold of $P < 0.05$. Scale bars, 5 cm (A–D), 50 μm (G) and (H). *Ch*, *C. hirsuta*; LL, lateral leaflet; TL, terminal leaflet; IR, inter-rachis.

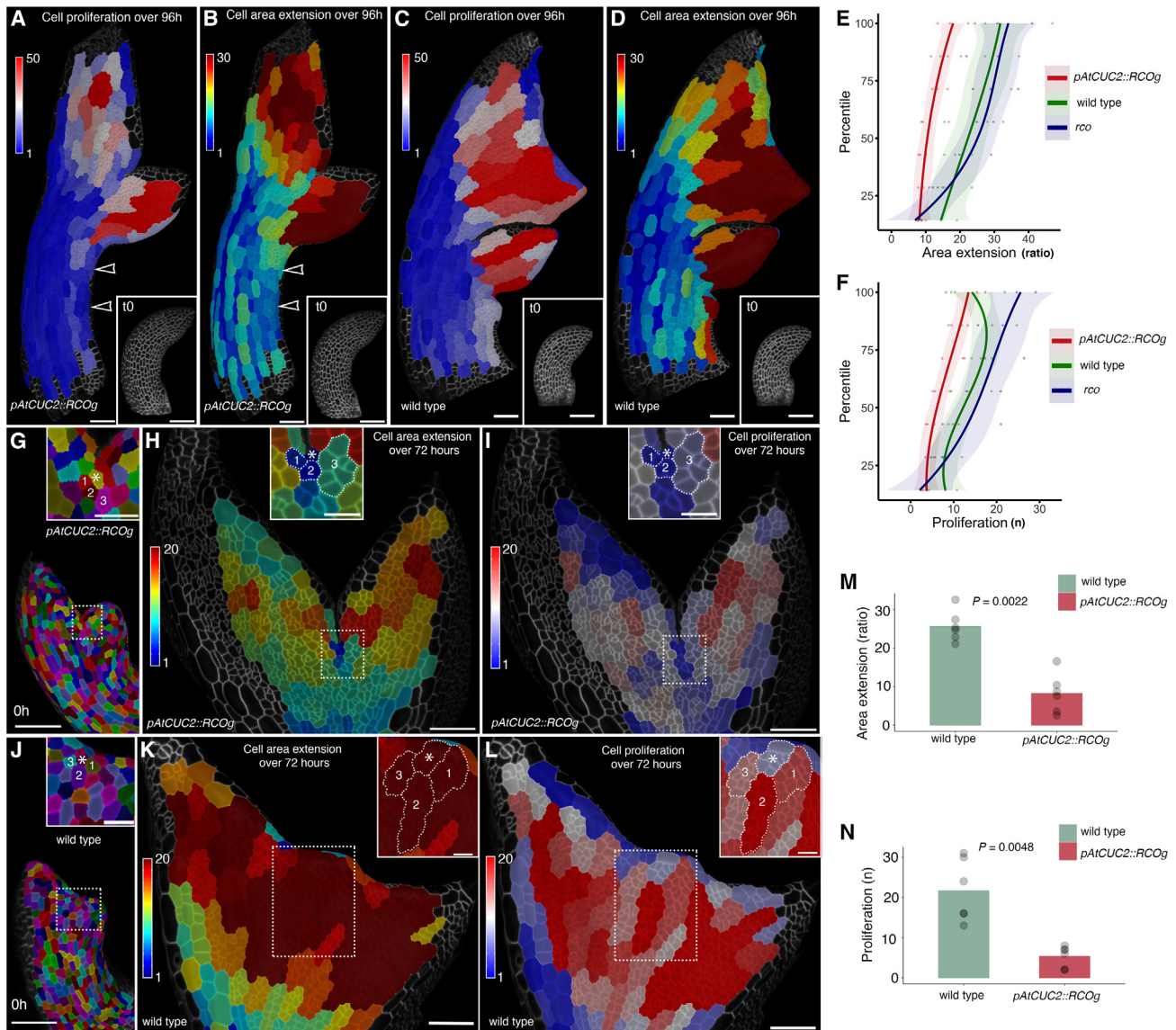


Figure 4. Forcing *RCO* in the *CUC2* domain alters cellular growth and proliferation patterns along the leaf margin

(A–D) Organ-wide heatmaps of cell proliferation (A) and (C) and cell area extension (B) and (D) in leaf 5 of *C. hirsuta* wild type carrying *pAtCUC2::RCOg* transgene (referred to as *pAtCUC2::RCOg* hereafter) (A) and (B) and *C. hirsuta* wild type (C) and (D) between 0 and 96 h. Insets in (A–D) show initial time point (0 h) at the start of the time-lapse.

(E and F) Alignment graphs of cell area extension (E) and cell proliferation (F) in *pAtCUC2::RCOg* (red, $n = 3$ time-lapse experiments), wild type (green, $n = 3$ time-lapse experiments), and *rco* mutant (blue, $n = 2$ time-lapse experiments) between 0 h (t_0) and 96 h (t_4) (over 5 days).

(G–L) Segmented meshes of the TL of *pAtCUC2::RCOg* (G) and wild type (J) at 0 h. Insets in (G) and (J) show close ups of sinus regions outlined in dotted rectangles. White asterisks in insets in (G) and (J) indicate landmark cells (and their neighbors, numbered) were analyzed for growth. Heatmaps of cell area extension in the sinus region of the TL of *pAtCUC2::RCOg* (H) and wild type (K). Insets in (H) and (K) show close ups of cellular growth in decedents of cells in insets of (G) and (J), respectively. Heatmaps of cell proliferation in the sinus region of the TL of *pAtCUC2::RCOg* (I) and wild type (L). Insets in (I) and (L) show close-ups of cellular proliferation in decedents of cells in insets of (G) and (J), respectively.

(M and N) Quantifications of cell area extension (M) and proliferation (N) in cellular clones shown in (G–L) over 72 h ($n = 2$ time-lapse experiments). Statistical significance was tested using Wilcoxon test with a significance threshold of $P < 0.05$. Scale bars, 50 μm (A–D) and (G–L), 10 μm (insets in G–L). *Ch*, *C. hirsuta*; *At*, *A. thaliana*; TL, terminal leaflet.

See also [Figures S3](#) and [S5](#) and [Video S3](#).

in vertebrate limb buds, inhibition of Sonic hedgehog (SHH) signaling disrupts the cell cycle and proliferative expansion of digit progenitor cells, causing a reduction in the number of digits.^{24,25} Also, in vertebrate tooth germs, loss of the

activity of muscle segment homeodomain proteins (MSX) causes a reduction in tooth number due to impaired proliferation in dental progenitor cells.^{26,27} Although fundamental aspects of development differ between plants and animals; for

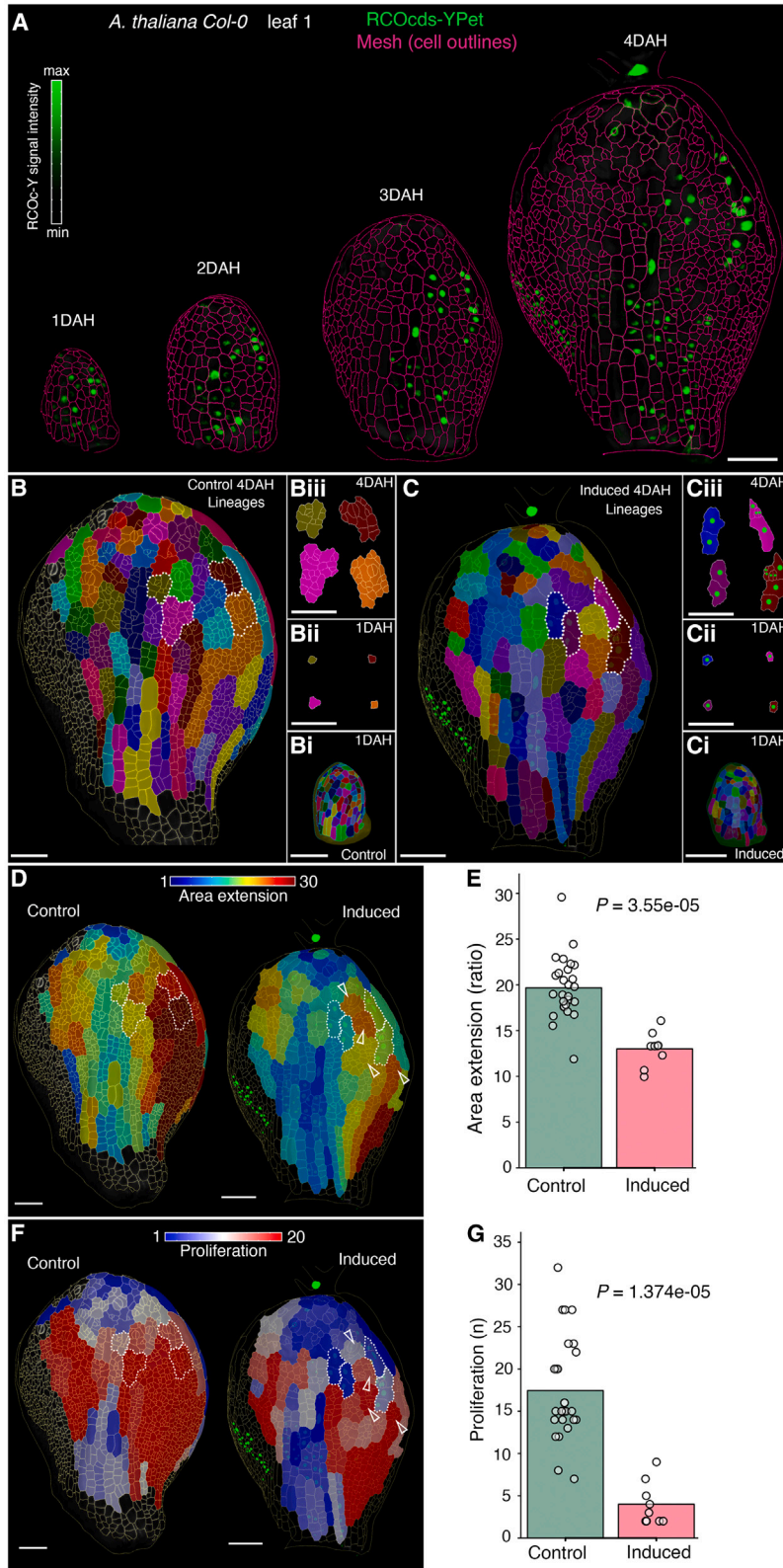


Figure 5. Genetic mosaics indicate that *RCO* is sufficient to restrict cell proliferation and cellular growth in a cell-autonomous manner

(A) Surface segmented meshes of *A. thaliana* leaf 1 showing cell outlines (magenta) and projected signal of RCO_{cds}-YPet clones (green).

(B and C) Leaf cell-fate maps of a control sample that was heat shocked (B) and of a leaf where RCO_{cds}-YPet sectors were induced upon heat shock (C). Colored clones in (B) and (C), at 4 day after heat shock (DAH), originate from same-colored cells at 1 DAH in (Bi) and (Ci), respectively. (Bii) and (Cii) show cells extracted from the segmented meshes at equivalent positions at 1 DAH in (Bi, control) and (Ci, induced), respectively. Green dots in (Cii) mark RCO_{cds}-YPet-expressing cells. (Biii) and (Ciii) show lineages of (Bii, control) and (Cii, induced), respectively, at 4 DAH, as also outlined in dotted polygons in complete meshes shown in (B) and (C).

(D–G) Heatmaps of cell area extension (D) and proliferation (F) in control and RCO_{cds}-YPet induced leaves between 1 DAH and 4 DAH. Note a reduction in cell proliferation and area extension in RCO_{cds}-YPet-expressing clones, compared with cells at an equivalent position in control samples (compare heatmap intensity in cells outlined with dotted polygons in control and induced). Quantification of cell area extension (E) and cell proliferation (G) in control and RCO_{cds}-YPet induced leaves between 1 DAH and 4 DAH. $n = 9$ RCO_{cds}-YPet clones from 3 induction and time-lapse experiments; each RCO_{cds}-YPet clone compared against 3 non-RCO-expressing clones at equivalent position in control ($n = 3$ time-lapse experiments). White arrowheads in (D) and (F) indicate relatively increased cell growth and proliferation in the neighboring cells of RCO_{cds}-YPet-expressing clones than the RCO_{cds}-YPet-expressing clones (see also Figures S4I and S4J). Statistical significance was tested using a linear regression model in (E) and a generalized linear regression model in (G) with a significance threshold of $P < 0.05$. Scale bars, 50 μm (A–C), (D), and (F). DAH, days after heatshock. See also Figures S4 and S5.

example, the plant cell wall cements cells in place and regulation of its extensibility is pivotal for turgor-driven growth. In contrast with this, animal cells can migrate and are under very different biophysical constraints compared with plants.²⁸ However, our work indicates that in both cases the coordination of tissue growth and cell division behavior is important for organogenesis. It also demonstrates how complex leaf development offers an attractive system for exploring interactions between growth, patterning, and cell proliferation during organogenesis.

Our findings indicate that *RCO* acts largely in a cell-autonomous manner to limit cell proliferation and cellular growth (Figures 5D and 5F). However, given that plant cells are connected to each other through cell walls, in the future it will be important to understand how surrounding cells coordinate their growth with slow-growing neighbors that express *RCO* in its endogenous context, by conducting genetic mosaic analysis in *rco* mutants. In this context, it will also be important to identify specific downstream target genes through which *RCO* acts to limit cell proliferation and growth, and to understand how these two facets of *RCO* action are mechanistically coordinated. One candidate is the cytokinin (CK) hormone pathway, which was previously shown to partially mediate *RCO* effects in leaf shape¹² and is also known to antagonize auxin signaling in different developmental contexts.²⁹ For example, CK has been shown to arrest the cycling of the pericycle founder cells in roots, thereby inhibiting the initiation of lateral root primordia,³⁰ which is conceptually similar to the effects of *pCUC2::RCO* on LL emergence. However, the developmental effects of CK are highly context dependent and involve both positive and negative effects on tissue growth at different stages of leaf development.³¹ Therefore, a thorough understanding of the molecular and cellular basis of CK action during leaf morphogenesis will be an important follow-up to this study.

STAR★METHODS

Detailed methods are provided in the online version of this paper and include the following:

- KEY RESOURCES TABLE
- RESOURCE AVAILABILITY
 - Lead contact
 - Materials availability
 - Data and code availability
- EXPERIMENTAL MODEL AND SUBJECT DETAILS
 - Plant growth conditions
- METHOD DETAILS
 - Cloning and generation of transgenic plants
 - Quantitative RT PCR
 - Sample preparation and live imaging
 - Image analysis and growth quantifications
 - Leaf phenotype analysis
- QUANTIFICATION AND STATISTICAL ANALYSIS

SUPPLEMENTAL INFORMATION

Supplemental information can be found online at <https://doi.org/10.1016/j.cub.2023.06.037>.

ACKNOWLEDGMENTS

We thank Dr. Marcus Heisler and Dr. Carolyn Ohno (The University of Sydney) for sharing constructs for creating genetic mosaics and YPet fluorescent protein. We thank Dr. Peter Huijser for help with phenotypic analysis, Rita Pabst for technical assistance, and Carla Galinha for help with generating materials. We also thank Dr. Angela Hay for providing critical feedback on the manuscript. This work was supported by a core grant from the Max Planck Society to M.T., the DFG Plant Morphodynamics (FOR2581) research unit to M.T., and an EMBO long-term fellowship ALTF-43-2019 to N.B.

AUTHOR CONTRIBUTIONS

N.B. performed most experiments and the majority of the data analysis; N.B. and M.T. designed the experiments and interpreted the results; N.B., D.W.-S., F.V., L.R.-L., and Z.H. contributed to material generation; S.S. developed R-scripts for generating growth alignment graphs and averaging CUC2-V expression; B.P. contributed to statistical analysis; N.B. and M.T. wrote the manuscript, with input from S.S., B.P., and D.W.-S.; M.T. designed and directed the study.

DECLARATION OF INTERESTS

The authors declare no competing interests.

INCLUSION AND DIVERSITY

We support inclusive, diverse, and equitable conduct of research.

Received: April 25, 2023

Revised: June 12, 2023

Accepted: June 13, 2023

Published: July 14, 2023

REFERENCES

1. Coen, E., Rolland-Lagan, A.G., Matthews, M., Bangham, J.A., and Prusinkiewicz, P. (2004). The genetics of geometry. *Proc. Natl. Acad. Sci. USA* *101*, 4728–4735. <https://doi.org/10.1073/pnas.0306308101>.
2. Gunawardena, A.H.L.A.N., and Dengler, N.G. (2006). Alternative modes of leaf dissection in monocotyledons. *Bot. J. Linn. Soc.* *150*, 25–44. <https://doi.org/10.1111/j.1095-8339.2006.00487.x>.
3. Kierzkowski, D., Runions, A., Vuolo, F., Strauss, S., Lymbouridou, R., Routier-Kierzkowska, A.L., Wilson-Sánchez, D., Jenke, H., Galinha, C., Mosca, G., et al. (2019). A growth-based framework for leaf shape development and diversity. *Cell* *177*, 1405–1418.e17. <https://doi.org/10.1016/j.cell.2019.05.011>.
4. Nikovics, K., Blein, T., Peaucelle, A., Ishida, T., Morin, H., Aida, M., and Laufs, P. (2006). The balance between the *MIR164A* and *CUC2* genes controls leaf margin serration in *Arabidopsis*. *Plant Cell* *18*, 2929–2945. <https://doi.org/10.1105/tpc.106.045617>.
5. Aida, M., Ishida, T., Fukaki, H., Fujisawa, H., and Tasaka, M. (1997). Genes involved in organ separation in *Arabidopsis*: an analysis of the *cup-shaped cotyledon* mutant. *Plant Cell* *9*, 841–857. <https://doi.org/10.1105/tpc.9.6.841>.
6. Barkoulas, M., Hay, A., Kougioumoutzi, E., and Tsiantis, M. (2008). A developmental framework for dissected leaf formation in the *Arabidopsis* relative *Cardamine hirsuta*. *Nat. Genet.* *40*, 1136–1141. <https://doi.org/10.1038/ng.189>.
7. Bilsborough, G.D., Runions, A., Barkoulas, M., Jenkins, H.W., Hasson, A., Galinha, C., Laufs, P., Hay, A., Prusinkiewicz, P., and Tsiantis, M. (2011). Model for the regulation of *Arabidopsis thaliana* leaf margin development. *Proc. Natl. Acad. Sci. USA* *108*, 3424–3429. <https://doi.org/10.1073/pnas.1015162108>.
8. Blein, T., Pulido, A., Vialette-Guiraud, A., Nikovics, K., Morin, H., Hay, A., Johansen, I.E., Tsiantis, M., and Laufs, P. (2008). A conserved molecular

- framework for compound leaf development. *Science* 322, 1835–1839. <https://doi.org/10.1126/science.1166168>.
- Sicard, A., Thamm, A., Marona, C., Lee, Y.W., Wahl, V., Stinchcombe, J.R., Wright, S.I., Kappel, C., and Lenhard, M. (2014). Repeated evolutionary changes of leaf morphology caused by mutations to a homeobox gene. *Curr. Biol.* 24, 1880–1886. <https://doi.org/10.1016/j.cub.2014.06.061>.
 - Vlad, D., Kierzkowski, D., Rast, M.I., Vuolo, F., Dello Ioio, R., Galinha, C., Gan, X., Hajheidari, M., Hay, A., Smith, R.S., et al. (2014). Leaf shape evolution through duplication, regulatory diversification, and loss of a homeobox gene. *Science* 343, 780–783. <https://doi.org/10.1126/science.1248384>.
 - Mentink, R.A., and Tsiantis, M. (2015). From limbs to leaves: common themes in evolutionary diversification of organ form. *Front. Genet.* 6, 284. <https://doi.org/10.3389/fgene.2015.00284>.
 - Hajheidari, M., Wang, Y., Bhatia, N., Vuolo, F., Franco-Zorrilla, J.M., Karady, M., Mentink, R.A., Wu, A., Oluwatobi, B.R., Müller, B., et al. (2019). Autoregulation of RCO by low-affinity binding modulates cytokinin action and shapes leaf diversity. *Curr. Biol.* 29, 4183–4192.e6. <https://doi.org/10.1016/j.cub.2019.10.040>.
 - Liao, C.Y., Smet, W., Brunoud, G., Yoshida, S., Vernoux, T., and Weijers, D. (2015). Reporters for sensitive and quantitative measurement of auxin response. *Nat. Methods* 12, 207–210. <https://doi.org/10.1038/nmeth.3279>.
 - Sauer, B. (1987). Functional expression of the cre-lox site-specific recombination system in the yeast *Saccharomyces cerevisiae*. *Mol. Cell. Biol.* 7, 2087–2096. <https://doi.org/10.1128/mcb.7.6.2087-2096.1987>.
 - Fox, S., Southam, P., Pantin, F., Kennaway, R., Robinson, S., Castorina, G., Sánchez-Corrales, Y.E., Sablowski, R., Chan, J., Grieneisen, V., et al. (2018). Spatiotemporal coordination of cell division and growth during organ morphogenesis. *PLoS Biol.* 16, e2005952. <https://doi.org/10.1371/journal.pbio.2005952>.
 - Neufeld, T.P., de la Cruz, A.F., Johnston, L.A., and Edgar, B.A. (1998). Coordination of growth and cell division in the *Drosophila* wing. *Cell* 93, 1183–1193. [https://doi.org/10.1016/s0092-8674\(00\)81462-2](https://doi.org/10.1016/s0092-8674(00)81462-2).
 - Boehm, B., Westerberg, H., Lesnicar-Pucko, G., Raja, S., Rautschka, M., Cotterell, J., Swoger, J., and Sharpe, J. (2010). The role of spatially controlled cell proliferation in limb bud morphogenesis. *PLoS Biol.* 8, e1000420. <https://doi.org/10.1371/journal.pbio.1000420>.
 - Lopez-Rios, J., Speziale, D., Robay, D., Scotti, M., Osterwalder, M., Nusspaumer, G., Galli, A., Holländer, G.A., Kmita, M., and Zeller, R. (2012). GLL3 constrains digit number by controlling both progenitor proliferation and BMP-dependent exit to chondrogenesis. *Dev. Cell* 22, 837–848. <https://doi.org/10.1016/j.devcel.2012.01.006>.
 - Vuolo, F., Kierzkowski, D., Runions, A., Hajheidari, M., Mentink, R.A., Gupta, M.D., Zhang, Z., Vlad, D., Wang, Y., Pecinka, A., et al. (2018). LMI1 homeodomain protein regulates organ proportions by spatial modulation of endoreduplication. *Genes Dev.* 32, 1361–1366. <https://doi.org/10.1101/gad.318212.118>.
 - Galbiati, F., Sinha Roy, D., Simonini, S., Cucinotta, M., Ceccato, L., Cuesta, C., Simaskova, M., Benkova, E., Kamiuchi, Y., Aida, M., et al. (2013). An integrative model of the control of ovule primordia formation. *Plant J.* 76, 446–455. <https://doi.org/10.1111/tpj.12309>.
 - Gonçalves, B., Hasson, A., Belcram, K., Cortizo, M., Morin, H., Nikovics, K., Vialette-Guiraud, A., Takeda, S., Aida, M., Laufs, P., et al. (2015). A conserved role for *CUP-SHAPED COTYLEDON* genes during ovule development. *Plant J.* 83, 732–742. <https://doi.org/10.1111/tpj.12923>.
 - Bhatia, N., Runions, A., and Tsiantis, M. (2021). Leaf shape diversity: from genetic modules to computational models. *Annu. Rev. Plant Biol.* 72, 325–356. <https://doi.org/10.1146/annurev-arplant-080720-101613>.
 - Efroni, I., Eshed, Y., and Lifschitz, E. (2010). Morphogenesis of simple and compound leaves: a critical review. *Plant Cell* 22, 1019–1032. <https://doi.org/10.1105/tpc.109.073601>.
 - Towers, M., Mahood, R., Yin, Y., and Tickle, C. (2008). Integration of growth and specification in chick wing digit-patterning. *Nature* 452, 882–886. <https://doi.org/10.1038/nature06718>.
 - Zhu, J., Nakamura, E., Nguyen, M.T., Bao, X., Akiyama, H., and Mackem, S. (2008). Uncoupling Sonic hedgehog control of pattern and expansion of the developing limb bud. *Dev. Cell* 14, 624–632. <https://doi.org/10.1016/j.devcel.2008.01.008>.
 - Han, J., Ito, Y., Yeo, J.Y., Sucov, H.M., Maas, R., and Chai, Y. (2003). Cranial neural crest-derived mesenchymal proliferation is regulated by Msx1-mediated p19(INK4d) expression during odontogenesis. *Dev. Biol.* 261, 183–196. [https://doi.org/10.1016/s0012-1606\(03\)00300-2](https://doi.org/10.1016/s0012-1606(03)00300-2).
 - Kero, D., Vukojevic, K., Stazic, P., Sundov, D., Mardesic Brakus, S., and Saraga-Babic, M. (2017). Regulation of proliferation in developing human tooth germs by MSX homeodomain proteins and cyclin-dependent kinase inhibitor p19(INK4d). *Organogenesis* 13, 141–155. <https://doi.org/10.1080/15476278.2017.1358337>.
 - Etournay, R., Popović, M., Merkel, M., Nandi, A., Blasse, C., Aigouy, B., Brandl, H., Myers, G., Salbreux, G., Jülicher, F., et al. (2015). Interplay of cell dynamics and epithelial tension during morphogenesis of the *Drosophila* pupal wing. *eLife* 4, e07090. <https://doi.org/10.7554/eLife.07090>.
 - Schaller, G.E., Bishopp, A., and Kieber, J.J. (2015). The yin-yang of hormones: cytokinin and auxin interactions in plant development. *Plant Cell* 27, 44–63. <https://doi.org/10.1105/tpc.114.133595>.
 - Li, X., Mo, X., Shou, H., and Wu, P. (2006). Cytokinin-mediated cell cycling arrest of pericycle founder cells in lateral root initiation of *Arabidopsis*. *Plant Cell Physiol.* 47, 1112–1123. <https://doi.org/10.1093/pcp/pcj082>.
 - Skalák, J., Vercruyssen, L., Claeys, H., Hradilová, J., Černý, M., Novák, O., Plačková, L., Saiz-Fernández, I., Skaláková, P., Coppens, F., et al. (2019). Multifaceted activity of cytokinin in leaf development shapes its size and structure in *Arabidopsis*. *Plant J.* 97, 805–824. <https://doi.org/10.1111/tpj.14285>.
 - Rast-Somssich, M.I., Broholm, S., Jenkins, H., Canales, C., Vlad, D., Kwantes, M., Bilsborough, G., Dello Ioio, R., Ewing, R.M., Laufs, P., et al. (2015). Alternate wiring of a KNOX1 genetic network underlies differences in leaf development of *A. thaliana* and *C. hirsuta*. *Genes Dev.* 29, 2391–2404. <https://doi.org/10.1101/gad.269050.115>.
 - Segonzac, C., Nimchuk, Z.L., Beck, M., Tarr, P.T., Robatzek, S., Meyerowitz, E.M., and Zipfel, C. (2012). The shoot apical meristem regulatory peptide CLV3 does not activate innate immunity. *Plant Cell* 24, 3186–3192. <https://doi.org/10.1105/tpc.111.091264>.
 - Schindelin, J., Arganda-Carreras, I., Frise, E., Kaynig, V., Longair, M., Pietzsch, T., Preibisch, S., Rueden, C., Saalfeld, S., Schmid, B., et al. (2012). Fiji: an open-source platform for biological-image analysis. *Nat. Methods* 9, 676–682. <https://doi.org/10.1038/nmeth.2019>.
 - Strauss, S., Runions, A., Lane, B., Eschweiler, D., Bajpai, N., Trozzi, N., Routier-Kierzkowska, A.L., Yoshida, S., Rodrigues da Silva, S., Vijayan, A., et al. (2022). Using positional information to provide context for biological image analysis with MorphoGraphX 2.0. *eLife* 11, <https://doi.org/10.7554/eLife.72601>.
 - Zhang, Z., Runions, A., Mentink, R.A., Kierzkowski, D., Karady, M., Hashemi, B., Huijser, P., Strauss, S., Gan, X., Ljung, K., et al. (2020). A WOX/auxin biosynthesis module controls growth to shape leaf form. *Curr. Biol.* 30, 4857–4868.e6. <https://doi.org/10.1016/j.cub.2020.09.037>.
 - (2021). R: A language and environment for statistical computing. R Foundation for Statistical Computing. https://scholar.google.com/scholar_lookup?title=R%3A%20A%20language%20and%20environment%20for%20statistical%20computing&publication_year=2021&author=R%20Core%20Team.
 - Elegant Graphics for Data Analysis (2016). (Springer-Verlag). https://link.springer.com/book/10.1007/978-3-319-24277-4?trk=public_post_comment-text.

39. Hay, A., and Tsiantis, M. (2006). The genetic basis for differences in leaf form between *Arabidopsis thaliana* and its wild relative *Cardamine hirsuta*. *Nat. Genet.* **38**, 942–947. <https://doi.org/10.1038/ng1835>.
40. Hay, A.S., Pieper, B., Cooke, E., Mandáková, T., Cartolano, M., Tattersall, A.D., Ioio, R.D., McGowan, S.J., Barkoulas, M., Galinha, C., et al. (2014). *Cardamine hirsuta*: a versatile genetic system for comparative studies. *Plant J.* **78**, 1–15. <https://doi.org/10.1111/tpj.12447>.
41. Lampropoulos, A., Sutikovic, Z., Wenzl, C., Maegele, I., Lohmann, J.U., and Forner, J. (2013). GreenGate—a novel, versatile, and efficient cloning system for plant transgenesis. *PLoS One* **8**, e83043, <https://doi.org/10.1371/journal.pone.0083043>.
42. Bhatia, N., Bozorg, B., Larsson, A., Ohno, C., Jönsson, H., and Heisler, M.G. (2016). Auxin acts through *MONOPTEROS* to regulate plant cell polarity and pattern phyllotaxis. *Curr. Biol.* **26**, 3202–3208. <https://doi.org/10.1016/j.cub.2016.09.044>.
43. Schmittgen, T.D., and Livak, K.J. (2008). Analyzing real-time PCR data by the comparative C(T) method. *Nat. Protoc.* **3**, 1101–1108. <https://doi.org/10.1038/nprot.2008.73>.
44. Strauss, S., Sapala, A., Kierzkowski, D., and Smith, R.S. (2019). Quantifying plant growth and cell proliferation with MorphoGraphX. *Methods Mol. Biol.* **1992**, 269–290. https://doi.org/10.1007/978-1-4939-9469-4_18.
45. Leigh, A., Sevanto, S., Close, J.D., and Nicotra, A.B. (2017). The influence of leaf size and shape on leaf thermal dynamics: does theory hold up under natural conditions? *Plant Cell Environ.* **40**, 237–248. <https://doi.org/10.1111/pce.12857>.
46. Cartolano, M., Pieper, B., Lempe, J., Tattersall, A., Huijser, P., Tresch, A., Darrah, P.R., Hay, A., and Tsiantis, M. (2015). Heterochrony underpins natural variation in *Cardamine hirsuta* leaf form. *Proc. Natl. Acad. Sci. USA* **112**, 10539–10544. <https://doi.org/10.1073/pnas.1419791112>.

STAR★METHODS

KEY RESOURCES TABLE

REAGENT or RESOURCE	SOURCE	IDENTIFIER
Chemicals, peptides, and recombinant proteins		
Sucrose	Sigma	Cat. #84097
Murashige and Skoog basal salt mixture	Sigma	Cat. #M5524
MES 2-(MN-morpholino)-ethane sulfonic acid	ROTH	Cat. #4256.4
Bacto Agar	ROTH	Cat. #5210.5
Murashige and Skoog Vitamin Solution	Sigma	Cat. #M3900
Plant Preservative Mixture (PPM)	Plant Cell Technology	Cat. #250
Propidium iodide (PI)	Sigma	Cat. #P4710
Mango Taq polymerase	Bioline	Cat. #BIO-21083
Phusion High-Fidelity DNA Polymerase	NEB	Cat. # M0530
In-Fusion® Snap Assembly Master Mix	Takara	Cat. # 638948
PrimeSTAR® GXL DNA Polymerase	Takara	Cat. #R050A
Gateway™ LR Clonase™ II Enzyme mix	Invitrogen™	Cat. #11791020
LR Clonase™ II Plus enzyme	Invitrogen™	Cat. # 12538120
Critical commercial assays		
RNeasy Plant Mini Kit	QIAGEN	Cat. #74904
SuperScript VILO cDNA Synthesis Kit	Invitrogen	Cat. #11754050
Power SYBR Green PCR Master Mix	Thermo Fisher Scientific	Cat. #4367659
Experimental models: Organisms/strains		
<i>C. hirsuta</i> ; <i>pChCUC2::ChCUC2g-VENUS</i> in wild type	Rast-Somssich et al. ³²	N/A
<i>C. hirsuta</i> ; <i>pChCUC2::ChCUC2g-VENUS</i> , <i>pChRCO::nls-tdTomato</i> in wild type	Generated in this study	N/A
<i>C. hirsuta</i> ; <i>pChRCO::RCOg-YPet-chrc3'utr</i> in <i>rco</i> mutant	Generated in this study	N/A
<i>C. hirsuta</i> ; <i>pAtCUC2::RCOg</i> in wild type	Generated in this study	N/A
<i>C. hirsuta</i> ; <i>pChCUC2::RCOg-YPet</i> in wild type	Generated in this study	N/A
<i>C. hirsuta</i> ; <i>pChCUC2::RCOcds-YPet</i> in wild type	Generated in this study	N/A
<i>C. hirsuta</i> ; <i>pChCUC2::RCOcds-YPet</i> in wild type	Generated in this study	N/A
<i>C. hirsuta</i> ; <i>pDR5v2::nls-3xVENUS</i> in wild type	Kierzkowski et al. ³	N/A
<i>C. hirsuta</i> ; <i>pAtCUC2::RCOg x pDR5v2::nls-3xVENUS</i> in wild type	Generated in this study	N/A
<i>C. hirsuta</i> ; <i>pChCUC2::RCOcds-YPet</i> in <i>rco</i> mutant	Generated in this study	N/A
<i>C. hirsuta</i> ; <i>pChCUC2::RCOcds-YPet</i> in wild type	Generated in this study	N/A
<i>C. hirsuta</i> ; <i>pChRCO::RCOcds-YPet</i> in <i>rco</i> mutant	Generated in this study	N/A
<i>C. hirsuta</i> ; <i>pDR5v2::nls-tdTomato</i> in wild type	Generated in this study	N/A
<i>C. hirsuta</i> ; <i>pChRCO::RCOcds-YPet x pDR5v2::nls-tdTomato</i> (<i>rco</i> mutant)	Generated in this study	N/A

(Continued on next page)

Continued

REAGENT or RESOURCE	SOURCE	IDENTIFIER
<i>C.hirsuta</i> ; pAtUBQ10::PM-YFP in <i>rco</i> mutant	Kierzkowski et al. ³	N/A
<i>C.hirsuta</i> ; pAtUBQ10::PM-tdTomato in wild type	Generated in this study	N/A
<i>C.hirsuta</i> ; pAtCUC2::RCOg x pAtUBQ10::PM-tdTomato (wild type)	Generated in this study	N/A
<i>A.thaliana</i> ; pHS::CRE-GR + p35S::lox-GUS-lox-RCOc-YPet in wild type	Generated in this study	N/A
<i>A.thaliana</i> ; pAtUBQ10::PM-tdTomato in wild type	Segonzac et al. ³³	N/A
<i>A.thaliana</i> ; pHS::CRE-GR + p35S::lox-GUS-lox-RCOc-YPet x pAtUBQ10::PM-tdTomato (wild type)	Generated in this study	N/A
<i>C.hirsuta</i> ; p35S::MIR164B; CUC3RNAi	Blein et al. ⁸	N/A
<i>C.hirsuta</i> ; pRCO::RCOg-VENUS	Kierzkowski et al. ³	N/A
<i>C.hirsuta</i> ; p35S::MIR164B; CUC3RNAi x pRCO::RCOg-VENUS	Generated in this study	N/A
Oligonucleotides		
All oligonucleotides	This Study	Table S1
Recombinant DNA		
p3.1kbAtCUC2::RCOg in pMLBart	This study	N/A
p2.6kbChCUC2::RCOcDs-YPet-2.6kb3'utr in pZP200BGW	This study	N/A
p2.6kbChCUC2::RCOg-YPet-2.6kb 3'utr in pZP200BGW	This study	N/A
p3.2kbChRCO::RCOg-YPet-1.2kb3'utr in pZP200BGW	This study	N/A
p3.2kbChRCO::RCOcDs-YPet-1.2kb3'utr in pZP200BGW	This study	N/A
p3.2kbChRCO::nls-tdTomato in pMLHyg	This study	N/A
pDR5v2::nls-tdTomato in pZP200 (Basta)	This study	N/A
pHS::CRE-GR + p35S::lox spacer lox::RCOcDs-YPet in pZP200BGW	This study	pHS::CRE-GR (in pBJ36); p35S::lox spacer lox (in pBJ36) vectors were gifted by Dr. Carolyn Ohno and Dr. Marcus Heisler
p3.2kbRCO::RCOg-VENUS-ocs in pMLBart	Kierzkowski et al. ³	N/A
Software and algorithms		
Leica application suite X	Leica	https://www.leica-microsystems.com/products/microscope-software/p/leica-las-x-ls/
Fiji (ImageJ 1.53q)	Schindelin et al. ³⁴	https://fiji.sc/
MorphoGraphX (MGX) (version 2.0)	Strauss et al. ³⁵	https://morphographx.org
Leaf Interrogator (LeafI)	Zhang et al. ³⁶	https://gitlab.mpcdf.mpg.de/g-adamrונים/leafinterrogator_zhang_et_al
R (version 4.2.2)	R Core team ³⁷	https://www.r-project.org/
R package: ggplot2	Wickham et al. ³⁸	https://ggplot2.tidyverse.org/
Imaris Viewer	OXFORD INSTRUMENTS	https://imaris.oxinst.com/imaris-viewer

RESOURCE AVAILABILITY

Lead contact

Further information and requests for resources and reagents should be directed to and will be fulfilled by the lead contact, Milto Tsiantis (tsiantis@mpipz.mpg.de).

Materials availability

All unique/stable reagents generated in this study will be made available from the lead contact with a completed Materials Transfer Agreement.

Data and code availability

- Microscopy data reported in this paper will be shared by the lead contact upon request.
- This paper does not report original code.
- Any additional information required to reanalyze the data reported in this paper is available from the lead contact upon request.

EXPERIMENTAL MODEL AND SUBJECT DETAILS

All transgenic lines were generated in *Cardamine hirsuta* (*Ch*) Oxford strain,³⁹ *rco* mutant¹⁰ and *Arabidopsis thaliana* (*At*, *Col-0* strain) background.

Plant growth conditions

Plants were grown in soil in greenhouses or in climate control chambers under long-day conditions (16-hour light: 8-hour dark, light intensity was $\sim 80\text{--}110 \mu\text{mol m}^{-2} \text{s}^{-1}$) at 22°C during day and 20°C during night. For phenotyping, all plants were cultivated in climate-controlled conditions mentioned above. For live imaging and time lapse experiments, seeds were surface sterilized in 70% ethanol (15 minute for *A. thaliana* and 30 minutes for *C. hirsuta*), sown on square petri dishes with GM medium (per liter- 10g sucrose (Sigma 84097), 4.33g Murashige and Skoog basal salt mixture (sigma M5524), 0.5g MES 2-(MN-morpholino)-ethane sulfonic acid, 8g Bacto Agar, 1 mL MS vitamins (Sigma), pH 5.7 with 1 M potassium hydroxide solution) and stratified in 4 degrees. Plates were then transferred to growth chamber under long-day conditions (16-hour light: 8-hour dark, light intensity was $\sim 80 \mu\text{mol m}^{-2} \text{s}^{-1}$) at 18°C.

METHOD DETAILS

Cloning and generation of transgenic plants

All transgenic lines were generated via floral dipping method⁴⁰ for both *Arabidopsis thaliana* and *Cardamine hirsuta*, using *Agrobacterium tumefaciens* strain GV3101. Oligos used for generating constructs are listed in Table S1.

pAtCUC2::RCOg construct was generated by amplifying 3.1kb of *AtCUC2* promoter and 1692bp of *RCOg* fragment and subcloning into *pBJ36*, upstream of the *ocs* terminator via an infusion reaction (Takara) using *EcoR1* and *BamH1* restriction site. The assembled *pAtCUC2::RCOg-ocs* fragment was subcloned into *pMLBart* via *Not1* site.

For generating *p2.6kbChCUC2::RCOg-YPet-2.6kb3'utr* and *p2.6kbChCUC2::RCOcds-YPet-2.6kb 3'utr ,9x alanine linker (polyA) and YPet* fragment was amplified and cloned into *pUC57* carrying multiple cloning site (mcs) flanked by *attL1* and *attL2* recombination sites (synthesized by GenScript) through infusion cloning at *BamH1* and *Xba1* restriction sites. *RCOgenomic* (1689bp, without stop codon) or *RCOcds* (648bp, without stop codon) were amplified without the stop codon and cloned upstream of *polyA-YPet* via infusion cloning at *BamH1* site. The *RCOg-polyA-YPet/ RCOc-polyA-YPet* translational fusions were cloned into a gateway binary vector carrying 2.6kb *ChCUC2* 5' regulatory sequence, *attR1*, *attR2*, 2.6kb *3'utr* and the *basta* resistance gene (synthesized by GenScript) via single LR reaction. The constructs were transformed into *Ch* wild type plants.

For generating *p3.2kbChRCO::RCOg-YPet-1.2kb3'utr* and *p3.2kbChRCO::RCOcds-YPet-1.2kb3'utr*, the *RCOg-polyA-YPet/ RCOc-polyA-YPet* translational fusions described above were cloned into a gateway binary vector carrying 3231bp *ChRCO* 5' regulatory sequence, *attR1*, *attR2*, 1212bp *3'utr* and *basta* resistance gene (synthesized by GenScript) via single LR reaction. The constructs were transformed into *rco* ems mutants described previously.¹⁰

For creating *pChRCO::nls-tdTomato*, *nls-tdTomato* was amplified and cloned into *pBJ36* at *HindIII* and *Xba1* restriction sites. Next, 3231bp *ChRCO* 5' regulatory sequence was amplified and cloned upstream of *nls-tdTomato* in *pBJ36* using *Xho1* and *Xma1* restriction enzymes. The resultant transcriptional fusion was subcloned into *pMLHyg* binary vector at *Not1* restriction site. The resultant construct was transformed into *Ch* wild type plants carrying *pChCUC2::ChCUC2genomic-VENUS* reporter.³²

pDR5v2::nls-tdTomato in *C. hirsuta* wild type was a kind gift from Dr. Angela Hay. Briefly, the plasmid was constructed by combining individual modules carrying- *pDR5v2*,¹³ *nls*, *tdTomato* and *RBCS* terminator sequence in a *basta* resistance binary vector using the Greengate cloning approach.⁴¹

To generate *p2.6kbChCUC2::RCOcds-YPet-2.6kb 3'utr* and *pDR5v2::nls-tdTomato* double reporter in *rco* mutant background, *C. hirsuta* wild type plants expressing *pDR5v2::nls-tdTomato* were crossed to *rco* mutants expressing *p2.6kbChCUC2::RCOcds-YPet-2.6kb 3'utr*. Homozygous *rco* mutants expressing both transgenes were isolated via selfing and genotyping. *C. hirsuta* transgenic lines carrying *p35S::MIR164B*; *CUC3RNAi*⁸ and *pRCO::RCOg-VENUS*³ were generated by crossing. The *pRCO::RCOg-VENUS-ocster* reporter was constructed by amplifying 3.2kb of the *RCO* promoter and 1689bp of the *RCO* genomic fragment carrying introns and cloning upstream and in-frame with *VENUS*. Individual components were assembled in pBJ36 shuttle vector carrying *ocs* terminator. The assembled *pRCO::RCOgenomic-VENUS-ocs* construct was subcloned into *pMLbart* using the *Not1* restriction enzyme.

pAtCUC2::RCOg and *pAtUBQ10::PM-tdTomato* as well as *pAtCUC2::RCOg* and *pDR5v2::nls-3xVENUS*¹³ double reporters in *C. hirsuta* wild type were generated by crossing. Construction of *pAtUBQ10::PM-tdTomato* is described previously.³³

For *RCO* genetic mosaic analyses, *Cre-Lox*-based recombination system¹⁴ was used. *pHS::CRE-GR* and *p35S::lox-spacer-lox* template constructs were kindly gifted by Dr. Marcus Heisler. Constructs were based on a previously published system.⁴² *RCOcds-polyA-YPet* translational fusion was amplified and cloned into *p35S::lox-spacer-lox*; pBJ36 via a unique *BamH1* restriction site to generate *p35S::lox-spacer-lox::RCOcds-YPet*. *pHS::CRE-GR* and *p35S::lox spacer lox::RCOcds-YPet* were combined in *pBGW* binary vector using Gateway cloning approach (Invitrogen). The construct was then transformed into *At col-0* plants. Transgenic lines expressing *pHS::CRE-GR* and *p35S::lox-spacer-lox::RCOcds-YPet* were crossed to *At Col-0* plants expressing *pAtUBQ10::PM-tdTomato*.

Quantitative RT PCR

For the qPCR experiment shown in Figure S2D wild type *Ch* plants and wild type *Ch* plants carrying *pAtCUC2::RCOg* were cultivated on GM medium described above. Leaf primordia 5 (500 μm in size) were dissected for RNA extraction. Three biological replicates (15 leaf primordia each) and three technical replicates for each biological replicate for each genotype were used. The total RNA was extracted using Qiagen RNeasy Plant Mini Kit. The first strand cDNA was synthesized with 1 μg of RNA using oligo dT (20-mer) primers and SuperScript VILO cDNA Synthesis Kit (Invitrogen). Quantitative RT-PCR was performed on a QuantStudio 3 Real-Time PCR System (ThermoFisher Scientific) using Power SYBR Green PCR Master Mix (ThermoFisher Scientific). *RCO* transcript levels were normalized to *ChGAPDH* transcript levels. Data was analyzed using the $2^{-\Delta\Delta\text{CT}}$ method.⁴³ Oligos used are listed in Table S1.

Sample preparation and live imaging

C. hirsuta seedlings were dissected to remove cotyledons and older leaves to expose the leaf node of interest. For time-lapse experiments described in Figure 4, the leaf node 5 was used when leaf primordium was approximately 75-90 μm in length. Images were acquired at 24 hours intervals. For *RCO* mosaic analysis (Figure 5), *A. thaliana* seedlings carrying the *pHS::CRE-GR* + *p35S::lox-spacer-lox::RCOcds-YPet* transgene were germinated on GM medium supplemented with 10 μM dexamethasone. Seedlings aged 2.5 DAS (days after stratification) were heat shocked at 37°C for 1-2 hours. Control seedlings carrying *pAtUBQ10::PM-tdTomato* only, and without the *pHS::CRE-GR* + *p35S::lox-spacer-lox::RCOcds-YPet* transgene were subjected to similar treatment. Time lapse was initiated 1 day after heat-shock (DAH). After induction, seedlings were transferred to GM medium plates without dexamethasone. One cotyledon was removed to expose leaves 1 and 2. Leaves (abaxial surface) were imaged every 24 hours until 4 days after heat shock. When required, leaf samples were stained with propidium iodide (PI) (1mg/ml working solution in water) to visualize cell walls. Live imaging was performed on a Leica TCS-SP8 upright confocal laser-scanning microscope using hybrid detectors (HyDs) and a 25X water objective (N.A 0.95). Pixel format was set to either 514x514 or 1024 x 1024 (for high resolution images). Sections were spaced from 0.5 μm -1 μm apart depending on the stage of leaf samples. Scan speed was set to 400Hz. *VENUS* and *YPet* were imaged using argon laser with excitation wavelength 514nm and collection range of 520-550nm. *tdTomato* and PI fluorescence were imaged with 561nm excitation wavelength and collection range of 570-590nm.

Image analysis and growth quantifications

Confocal microscopy data were processed and visualized using Imaris viewer (OXFORD INSTRUMENTS), Image J (FIJI³⁴) and MorphoGraphX.³⁵ Quantification of signal intensities of *pChCUC2::ChCUC2g-V* and *pRCO::nls-tdTomato* shown in Figures 1D–1F was performed in MorphoGraphX. Samples were processed using standard procedures to create surface segmented meshes based on PI (cell wall) staining.⁴⁴ Then both *pChCUC2::ChCUC2g-VENUS* and *pRCO::nls-tdTomato* signals were projected onto the segmented meshes (from a distance of 2 μm - 12 μm under the mesh) to quantify cellular expression. Cells within a distance of 12 cells from the distal end of the lateral leaflet were included in the analysis to include all cells at the leaflet base and at junction between terminal and lateral leaflet. Signal intensities were visualized as heat maps and data was exported to csv files. Cells were classified into two groups in MorphoGraphX - *pChCUC2::ChCUC2g-VENUS* expression domain and *pRCO::nls-tdTomato* expression domain based on generated heat maps and cell distance from the leaflet tip. Signal intensities of *pChCUC2::ChCUC2g-VENUS* and *pRCO::nls-tdTomato* were plotted in each of these two groups.

Quantification of distances between DR5 expression foci (shown in Figures 3G–3I) was performed using MorphoGraphX. For this, leaf node 6 of plants grown in long day conditions on GM-vit medium (described above), with roughly similar length (650 μm -750 μm) and same number of visible *pDR5v2::nls-tdTomato* expression foci were used. Leaf length was measured using a manually placed Bezier curve, originating from leaf base and aligned with the curved leaf surface along the midrib upto the leaf tip using multiple

control points. To measure the distances between DR5 expression foci, we used multiple control points of a second Bezier curve that were manually placed at leaf tips and sinuses along the leaf margin. Instead of using the Bezier curve we now connected the control points with linear line segments and exported control point coordinates and line segment length from MorphoGraphX. Finally, distances between two expression foci were computed as a sum of the length of segments between the control points and plotted as a proportional distance of the sum of total length of all linear segments.

Cell fate mapping and cellular growth analysis shown in [Figures 4](#), [5](#), and [S3–S5](#) was performed using MorphoGraphX. Surface segmented organ meshes were generated by processing raw data using the standard procedure.⁴⁴ Surface cell fate maps were generated for all progressive time points and individual lineages were merged to obtain final fate maps of cells in the initial time point (t_{initial} to t_{final}). Incomplete lineages were not used for further analysis and cellular growth parameters of area extension and cell proliferation were quantified. Area extension was calculated as the ratio of cell area between the final and the initial timepoint (fold change).¹⁰ Cell proliferation was calculated as the number of cells at the final timepoint that originated from a single cell at the initial time point. Cell area extension and cell proliferation patterns between initial timepoint and the final timepoint were visualized using heatmaps projected onto the final timepoint.

For organ-wide comparison along the proximo-distal axis (between replicates for each genotype and between genotypes shown in [Figures 4E](#) and [4F](#)) growth alignment graphs were generated based on a positional coordinate system described previously.^{35,36} To create the alignment, cells at leaf bases were manually selected (corresponding to equivalent positions) in each leaf sample prior to shape divergence i.e., at the initial time point. Then for all cells their shortest path through cell centers to the selected leaf base was computed to obtain Euclidean cell distances from the leaf base. Cells were then split into 7 bins based on their distance values. Information of area extension and cell proliferation on each clone was calculated in MorphoGraphX and data was exported as a csv file. This data was used to generate growth alignment graphs and associated plots for statistical analysis shown in ([Figures S3A](#) and [S3B](#)) using custom R-scripts (as described in [Zhang et al.](#)³⁶). For dot box plots of cell proliferation and cell area extension shown in ([Figures S3C](#) and [S3D](#)), information from cells in bins 3–6, that were completely mapped on the final timepoint were used.

For clonal analysis shown in [Figures 4G–4N](#), a reference cell was manually selected in the sinus region of the terminal leaflet both genotypes, wild type and wild type expressing *pAtCUC2::RCOg* at the initial time point (marked in *). Next, 3 neighboring (non-marginal) cells in the immediate proximity to the reference cell, with complete lineages were chosen for analysis. A third replicate imaged slightly differently (starting at a younger stage and imaged every 24 hours until 96 hours in total) was subjected to same analysis and was found to show similar results.

For analysis of cell area extension and cell proliferation in leaves with RCOcbs-YPet mosaics and to compare those with control leaves, a positional coordinate system along the proximo-distal axis axis (as explained above) and medio-lateral axis (distance from the leaf margin) in combination with visual estimation was used to identify cells at equivalent positions in control and induced leaves ([Figures 5B](#) and [5C](#)). Only epidermal RCOcbs-YPet clones were used for analysis. Information of area extension and cell proliferation on each cellular clone was calculated in MorphoGraphX and data was exported to a csv file. This data was used to generate plots shown in [Figures 5E](#) and [5G](#). For graphs shown in [Figures S4I](#) and [S4J](#), an analysis of cell area extension and cell proliferation was conducted in RCOcbs-YPet expressing cells in comparison to their non-RCOcbs-YPet expressing neighbors. RCOcbs-YPet expressing clones were chosen such that they had at least 3 non-RCOc-YPet expressing immediate cell neighbors.

For data shown in [Figures S5A–S5M](#) we developed a landmark-based method to compute mean heat maps of multiple samples and to project heat maps onto different samples for curved surface meshes in MorphoGraphX. The goal was to examine the fate of *CUC2* expressing cells during leaflet outgrowth in the wild type plants, since our transgenic lines carrying dual reporters-*pChCUC2::ChCUC2g-VENUS* (*CUC2-V*) and *pUBQ10:PM-tdTomato* showed transgene silencing. For this, leaf primordia of plants expressing *pChCUC2::ChCUC2g-VENUS* only were stained with PI to visualize cell outlines and imaged at a stage prior to first leaflet emergence when the terminal leaflet protrusion was visible and the leaf margin at the site of lateral leaflet protrusion displayed a concave curvature. Images were processed in MorphoGraphX to create surface segmented meshes to generate *CUC2-V* intensity heatmaps. Heat maps from multiple samples ($n=3$) showed two *CUC2-V* expression foci, first in the sinus of the terminal leaflet and second in the region with concave margin curvature, below the terminal leaflet protrusion ([Figures S5A–S5C](#)). We aimed to create an average *CUC2-V* intensity heatmap from the three reference samples at a similar stage, which could be loaded and visualized as mapped heat values of *CUC2-V* expression on to time-lapsed samples at equivalent starting stage but without *pChCUC2::ChCUC2g-VENUS*. For this, five landmarks were assigned to each leaf primordium sample to create different positional coordinate system based on relative distances from cells at leaf tip, leaf base, midrib, sinus of the terminal leaflet protrusion and the center of the concave leaf margin curvature below the terminal leaflet protrusion.³⁵ The latter two were determined based on the computed tissue curvature to identify the cell at the center of the concave regions. Together with the *CUC2-V* expression those positional coordinate heat maps were exported to R, where a custom script was used to create an averaged/ mapped heat for *CUC2-V* expression for each target time-lapsed sample (segmented mesh). In brief, averaged heat values of *CUC2-V* for each cell in the target sample were computed using a weighted mean approach where the weights were determined by the distances in the positional coordinate of all cells in the other samples, similar to a mean squared error. This averaged/mapped heat expression was verified by loading mapped heat values on to each of the original *CUC2-V* expressing meshes and it resembled the corresponding original *CUC2-V* intensity heat maps for each sample. After verification, mapped/average heat values were loaded on to two different time-lapsed wild type leaf primordia starting at a similar stage to original *CUC2-V* expressing leaf samples ([Figures S5D–S5G](#)).

Leaf phenotype analysis

To quantify leaf margin complexity as shown in [Figure 2C](#), leaf silhouettes (leaf node 3-8) were obtained by flattening leaves collected from 4 weeks old plants onto transparent adhesive paper, and scanning to obtain black and white images. Resampled contours of the terminal leaflet (TL) were derived from whole leaf silhouettes using Leaf Interrogator (LeafI)³⁶ and were used to compute NDMC (Normalised differential margin complexity, defined by:⁴⁵

$$\left(\frac{\text{Perimeter of the contour} - \text{Perimeter of the convex hull}}{\text{Perimeter of the contour} + \text{Perimeter of the convex hull}} \right).$$

To compute inter-rachis (IR) length as shown in [Figure 3F](#), leaf silhouettes were obtained as described above. Inter-rachis length (distance between two leaflets along the rachis; Cartolano et al.⁴⁶) was measured using a custom-made macro in Fiji. Distances were measured on each side of the leaf margin, starting at the leaf base and normalized against the total rachis length (petiole+interrachis+terminal rachis). Each replicate (T2 line) of each genotype consisted of two leaves each (leaf node 7 and 8) from 8 plants. The proportional inter-rachis distances (percentages) were used to generate the density plot shown in [Figure 3F](#). Distributions of replicates within a genotype were checked and were found to be not different from each other.

QUANTIFICATION AND STATISTICAL ANALYSIS

Statistical analysis performed and number of replicates analyzed are specified in figure legends. All tests were performed in R. The significance threshold used was $P < 0.05$. In [Figures 5E](#) and [5G](#), regression analysis was used to test if the presence of RCO_{cds}-YPet and the location on the developing leaf had significant effects on cell growth and proliferation. For the continuous variable cell growth, a linear model was used that included location on the leaf. The effect of RCO_{cds}-YPet on cell growth was plotted using a derived variable where the effect of location in the leaf was regressed out. The cell count data quantifying proliferation was analyzed using a generalized linear model of the quasipoisson family to account for its overdispersion. The effect of RCO_{cds}-YPet on cell proliferation was plotted using the raw data because the location on the leaf did not affect this trait.